A Journal of the Gesellschaft Deutscher Chemiker
Angewandte
GDCh
International Edition
Chemie
www.angewandte.org

Accepted Article

Title: Modular Reconfigurable DNA Origami: from 2D to 3D

Authors: Yan Liu, Jin Cheng, Sisi Fan, Huan Ge, Tao Luo, Linlin Tang, Bin Ji, Chuan Zhang, Daxiang Cui, Yonggang Ke, and Jie Song

To be cited as: *Angew. Chem. Int. Ed.* 10.1002/anie.202010433

Link to VoR: https://doi.org/10.1002/anie.202010433

WILEY-VCH

10.1002/anie.202010433

WILEY-VCH

Research articles

Modular Reconfigurable DNA Origami: from 2D to 3D

Yan Liu [a]+, Jin Cheng [a]+, Sisi Fan [a]+, Huan Ge [b], Tao Luo [a], Linlin Tang [a], Bin Ji [a], Chuan Zhang [b], Daxiang Cui [a], Yonggang Ke [c], Jie Song [a, d]*

[a] Y. Liu [+], J. Cheng [+], S.S. Fan [+], T. Luo, L.L. Tang, B. Ji, Prof. D. Cui, Prof. J. Song
Institute of Nano Biomedicine and Engineering,
Department of Instrument Science and Engineering,
School of Electronic Information and Electrical Engineering,
Shanghai Jiao Tong University, Shanghai 200240, China.
E-mail: sjie@sjtu.edu.cn
[b] H. Ge, Prof. C. Zhang
School of Chemistry and Chemical Engineering,
Frontiers Science Center for Transformative Molecules,
State Key Laboratory of Metal Matrix Composites,
Shanghai Jiao Tong University, Shanghai 200240, China.
[c] Prof. Y.G. Ke
Wallace H. Coulter Department of Biomedical Engineering,
Georgia Institute of Technology and Emory University,
30322, Atlanta, GA, USA.
[d] Prof. J. Song
Institute of Cancer and Basic Medicine (IBMC), Chinese Academy of Sciences,
The Cancer Hospital of the University of Chinese Academy of Sciences, Hangzhou, Zhejiang 310022, China.
[+] These authors contributed equally to this work.

***Abstract*:** DNA origami has represented a novel route to manipulate objects at nanoscale, and demonstrated unprecedented versatility in fabricating both static and dynamic nanostructures. Here, we introduce a new strategy for transferring modular reconfigurable DNA nanostructures from 2D to 3D. A 2D DNA sheet could be modularized into connected parts (e.g. two, three and four parts in this work), which can be independently transformed between two conformations with a few DNA "trigger" strands. More interestingly, the transformation of the connected 2D modules can lead to the controlled, resettable structural conversion of a 2D sheet to a 3D architecture, due to the constraints induced by the connections between the 2D modules. This new approach can provide an efficient mean for constructing programmable, higher-order, and complex DNA objects, as well as sophisticated dynamic substrates for various applications.

Introduction

Since the concept of structural DNA nanotechnology was firstly demonstrated by Ned Seeman in 1982 [1], the field has flourished rapidly during the last decades, especially with the invention of DNA origami by Paul Rothemund in 2006 [2]. For DNA origami design, a long scaffold strand (typically a m13 viral genomic DNA, ~7k bases) is folded into a prescribed shape by interacting with ~100-200 synthetic "staple" strands. Until now, tremendous progress has been made for constructing static DNA origami from 1D [3], 2D [4] to 3D [5] objects with defined shapes, as well as dynamic DNA origami like tweezers [6], switches [7], walkers [8], circuits [9], nanorobots [10], and our previously reported "domino" nanoarrays [11]. However, it's worth noting that remodelling each origami involved de novo design and high cost of different staple strands, particularly dimensional variation of the nanostructures from 2D to 3D [12]. Therefore, more powerful capability of dynamically reconfigurable design strategy is needed for realizing more manifold applications, such as sensing [13], delivering nanomedicines [14], navigating the local environment [15], transferring motion [16], forces [17], and energy [18], and so on.

Herein, we demonstrated a modular transformation strategy based on the reconfigurable DNA origami nanoarray, realizing a controllable transformation of nanostructures from 2D to 3D. The reconfigurable DNA origami nanoarray was constructed through the self-assembly of small reconfigurable modular DNA blocks (also called anti-junction units), which could reconfigure from one conformation to another conformation. In addition, a 2D DNA sheet could be modularized into connected parts (e.g. two, three and four parts in this work), which can be modularly transformed. Furthermore, the modular transformation could realize resettable structural transformation between 2D and 3D nanostructures due to the shape change of the individual modules and the constraints induced by the connections between modules. This modular reconfigurable DNA origami strategy allows us to remodel the preformed DNA nanostructures, improving the sophistication and functionality of the nanoscale assemblies and nanorobots for various applications.

Results and Discussion

To demonstrate the strategy of constructing modular reconfigurable DNA nanostructures, we constructed a 2D reconfigurable DNA origami sheet firstly (Figure 1A). The reconfigurable DNA origami sheet composed of interconnected anti-junction units. The mobile nicking points at the boundary of the interconnected anti-junction units made it unstable. After adding the trigger DNA strands, the anti-junction units could convert between two independent conformations - "blue" and "red". Based on this principle, the reconfigurable DNA origami could transform from "blue" to "red" configuration or rectangle to square configuration by trigger DNA strands. In the previous work [11a], the transformation mainly focused on the continuous transformation of an entire nanostructure, and no

10.1002/anie.202010433

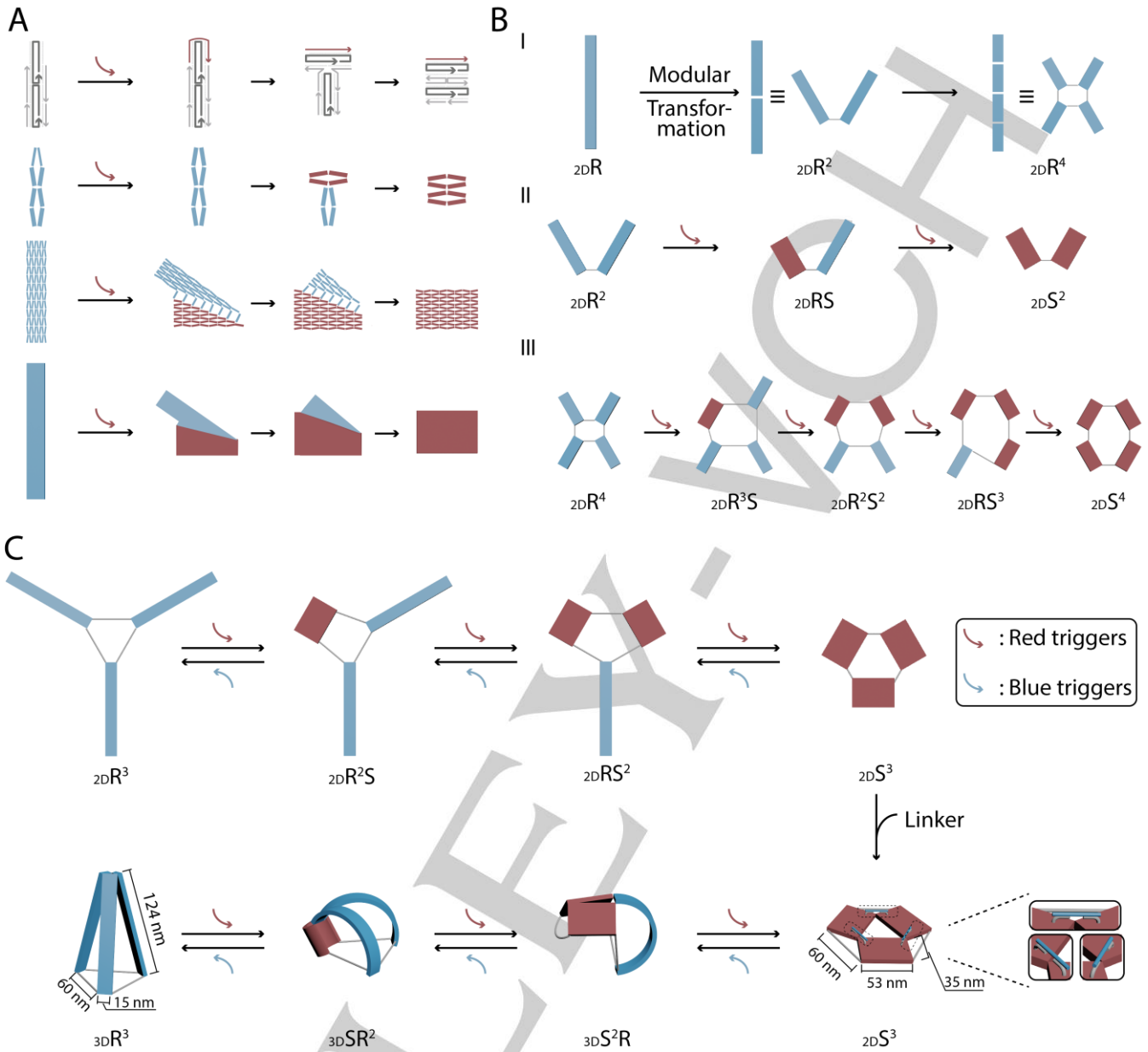

Figure 1. An overview of modular reconfigurable DNA nanostructures strategy. (A) Conformational transformation of the interconnected anti-junction units and 2D DNA origami. Note that the DNA origami is composed of multiple anti-junction units. (B). Modular transformation of 2D DNA origami. The original rectangle DNA origami ($_{2D}R$) could be modularized into two-rectangle nanostructure ($_{2D}R^2$) and four-rectangle nanostructure ($_{2D}R^4$). (C) Resettable structural conversion of a 2D sheet to a 3D architecture. The three-rectangle nanostructure ($_{2D}R^3$) could be independently transformed with different kinds of trigger DNA strands. With the help of linkers, the modular transformation could realize resettable structural transformation between 2D and 3D nanostructures, due to the constraints induced by the connections between the 2D modules.

stable intermediate states were intentionally designed in the structures, although intermediate states (e.g. the two intermediates in Figure 1A) of a structure could be occasionally observed in the imaging process. To realize modular transformation, we modified the 2D sheet origami to generate a two-rectangle DNA origami ($_{2D}R^2$) and a four-rectangle DNA origami ($_{2D}R^4$, Figure 1B). By adding different trigger DNA strands, the modular transformation of individual rectangles could be realized (Figure 1B). We then explored whether the modular transformation could lead to more complex reconfiguration of DNA origami, by carefully designing the connecting scheme of the modular units. To this end, a three-rectangle DNA origami ($_{2D}R^3$) was designed (Figure 1C). The three-part origami can realize a resettable transformation between two 2D conformations of $_{2D}R^3$ and $_{2D}S^3$. Red and blue trigger DNA strands were applied for the resettable structural transformation, and the functions of the two triggers were the same. The difference between the two triggers was that they acted on the different nicking points of the reconfigurable DNA origami sheet. Furthermore, with the addition of three linkers, the $_{2D}S^3$ was converted to tightened structure that can exhibit resettable, modular transformation between 2D conformation ($_{2D}S^3$) and 3D

10.1002/anie.202010433

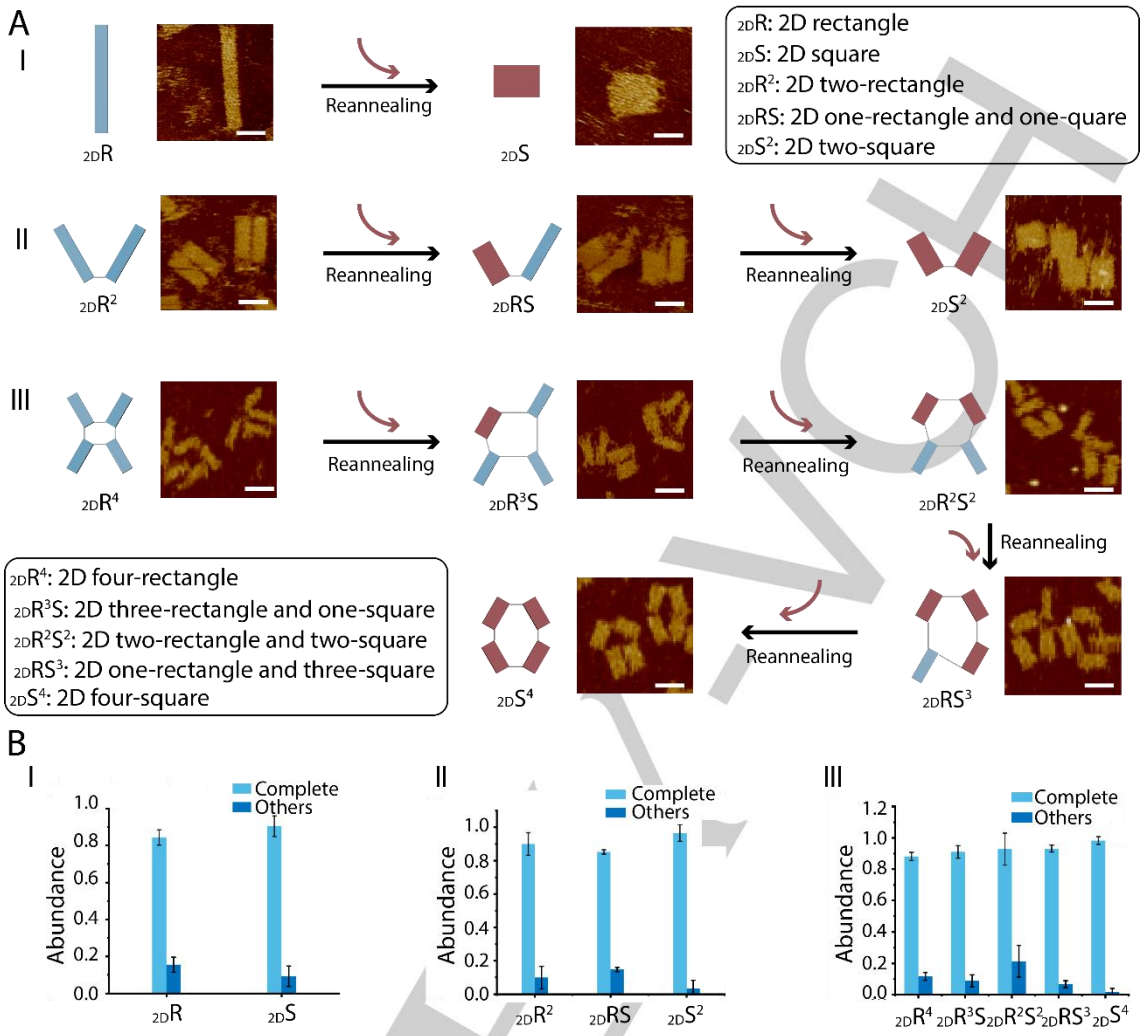

Figure 2. Controlled formation of 2D modular reconfigurable DNA origami. (A) Controlled formation of (I) $_{2D}$R DNA origami to 2D square DNA origami ($_{2D}$S), (II) $_{2D}$R^2 DNA origami to $_{2D}$S^2 DNA origami, and (III) $_{2D}$R^4 DNA origami to $_{2D}$S^4 DNA origami. (B) Yield analysis of the controlled formation of 2D modular DNA origamis. Scale bars: 50 nm.

conformations ($_{3D}$S^{2}R, $_{3D}$SR^2, $_{3D}$R^3), due to the shape change of the individual modules and the constraints induced by the connections between modules.

To demonstrate the feasibility and efficiency of the modular reconfigurable transformation strategy, we built a reconfigurable $_{2D}$R DNA origami for conceptual explanation firstly. The nanostructures were formed by a thermal annealing process, and 8 red triggers (100 nM/per trigger) were applied for the formation of the square nanostructures. The reconfigurable DNA origami could realize the controllable formation from the rectangle to square nanostructure by triggers, and the DNA origami was confirmed by atomic force microscope (AFM). In Figure 2A-I, the reconfigurable DNA origami could be structural programming from rectangle (190 × 30 nm) to square nanostructure (70 × 80 nm). Furthermore, $_{2D}$R^2 DNA origami and $_{2D}$R^4 DNA origami were designed to realize the manageable formation. These two DNA origamis were generated by modulating the original reconfigurable DNA origami in Figure 2A-I. As illustrated in Figure 2A-II and Figure 2A-III, the manageable formation in $_{2D}$R^2 DNA origami and $_{2D}$R^4 DNA origami was realized by adding different triggers. As shown in Figure 2A-II, the size of each modules was about 90 × 30 nm (rectangle) and 50 × 60 nm (square), respectively. When the original nanostructure was divided into four units, the rectangle modules (50 × 25 nm) could be formed to square modules (30 × 40 nm) driven by the triggers. Additionally, the maneuverable formation efficiency of different nanostructures was calculated (Figure 2B). We could obtain an efficient maneuverable formation between $_{2D}$R and $_{2D}$S with a yield over 80%. For the modular designs, the maneuverable formation efficiencies of the units in both the $_{2D}$R^2 DNA origami and $_{2D}$R^4 DNA origami were over 80% as well, suggesting that the controllable formation in 2D DNA origami could be successfully realized with high efficiency.

After realizing the maneuverable formation in $_{2D}$R^2 DNA origami and $_{2D}$R^4 DNA origami, we then explored whether the maneuverable formation of a 2D connected DNA origami could be realized. A new

10.1002/anie.202010433

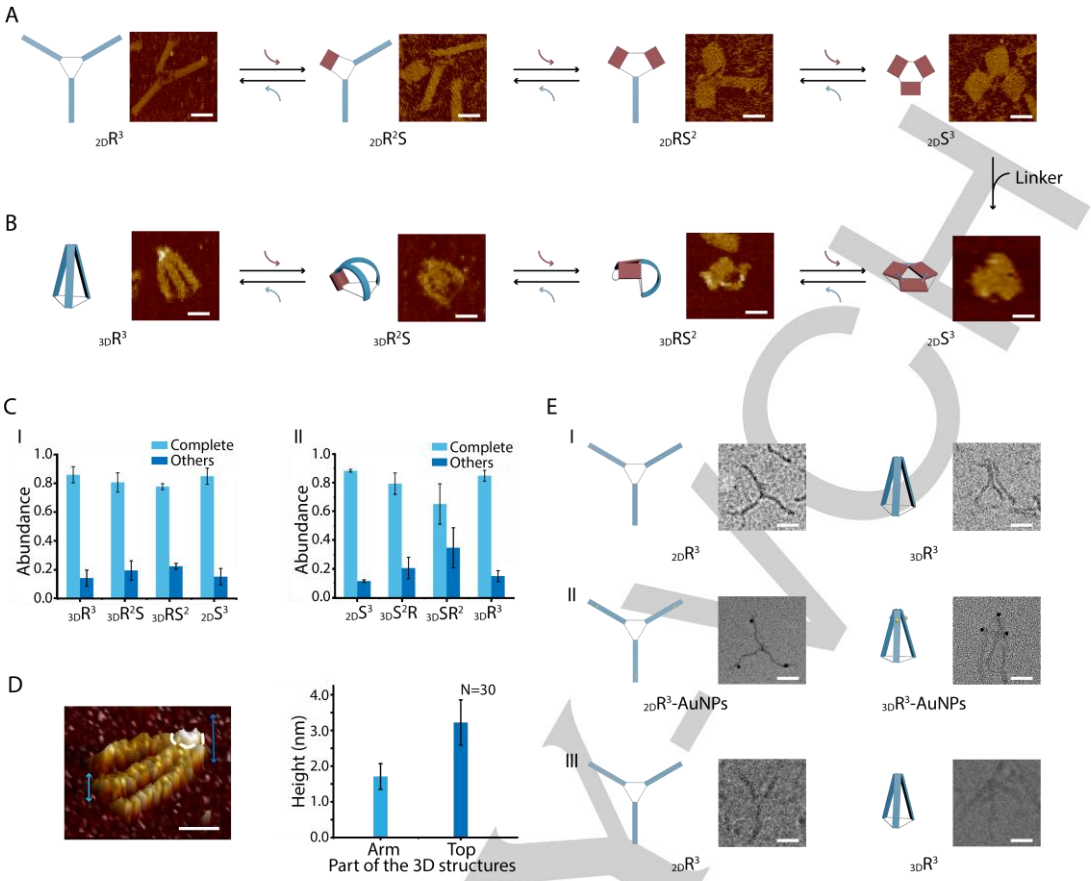

Figure 3. Controllable formation of 2D connected reconfigurable DNA origami. (A) Controllable formation between $_{2D}R^3$ and $_{2D}S^3$ nanostructures, and (B) between $_{3D}R^3$ connected nanostructures and $_{2D}S^3$ connected nanostructures. (C) Yield analysis of (I) $_{3D}R^3$ connected nanostructures to $_{2D}S^3$ connected nanostructures, and (II) $_{2D}S^3$ connected nanostructures to $_{3D}R^3$ connected nanostructures. (D) Height analysis of $_{3D}R^3$. (E) Characterization of the $_{2D}R^3$ and $_{3D}R^3$ nanostructures. TEM characterization of (I) $_{2D}R^3$ and $_{3D}R^3$ connected nanostructures, (II) $_{2D}R^3$-AuNPs and $_{3D}R^3$-AuNPs nanostructures (AuNPs: 5 nm). Note that $_{2D}R^3$-AuNPs meant that gold nanoparticles were bonded with the nanostructures. (III) Cryo-EM characterization of $_{2D}R^3$ and $_{3D}R^3$ nanostructures. Left: $_{2D}R^3$ connected nanostructures, right: $_{3D}R^3$ connected nanostructures. All the nanostructures were formed by a thermal annealing process. Scale bars: 50 nm.

$_{2D}R^3$ DNA origami was designed in Figure 3. Firstly, controllable formation of the $_{2D}R^3$ DNA origami was realized. The same as Figure 2, the formation between $_{2D}R^3$ and $_{2D}S^3$ DNA origami occurred with nanostructures binding different triggers (Figure 3A). At the same time, the formation efficiency was over 80% (Figure S21 and S27). According to our design, the linkers could be applied to connect and tighten up the adjacent square nanostructures. The tightened $_{2D}S^3$ nanostructure was employed to explore whether the connected DNA nanostructure could realize a modular transformation and dimensional transformation from 2D to 3D. As seen in Figure 3B, the controllable formation between 2D and 3D was successfully realized with the help of different triggers. Meanwhile, the controllable formation efficiency between 2D and 3D was also calculated with the yield over 80% (Figure 3C, Figure S35-S38 and Figure S40-S43). As shown in Figure 3D, the junction part of the $_{3D}R^3$ DNA origami presented the height over 3 nm, which further demonstrated the 3D architecture. To further clarify and prove the 3D nanostructure, transmission electron microscope (TEM) and cryogenic electron microscope (cryo-EM) were applied to characterize the $_{2D}R^3$ and $_{3D}R^3$ nanostructures (Figure 3E). Figure 3E-I showed the TEM of $_{2D}R^3$ and $_{3D}R^3$ connected nanostructures. To get a better understanding of the 3D nanostructures, gold nanoparticles (AuNPs) were bonded with $_{2D}R^3$ and $_{3D}R^3$ nanostructures. The assemblies of $_{2D}R^3$-AuNPs and $_{3D}R^3$-AuNPs were characterized by TEM after agarose gel purification. According to the mechanism of 2D to 3D transformation, AuNPs was linked as the top of the $_{3D}R^3$ nanostructures, and the representative TEM images showed the effective assemblies between the AuNPs and $_{3D}R^3$ nanostructures (Figure 3E-II). In contrast with $_{2D}R^3$-AuNPs nanostructures, the linking of the AuNPs and $_{3D}R^3$ nanostructures could further demonstrated the formation of the 3D nanostructures. To further confirm and show the 3D nanostructures more actually, the folded $_{2D}R^3$ and $_{3D}R^3$ nanostructures were analyzed by cryo-EM. Figure 3E-III showed representative cryo-EM images. Interestingly, the size of the whole $_{3D}R^3$ nanostructures narrowed in the vertical view (Figure S46), which more clearly demonstrated that the $_{3D}R^3$ nanostructures were 3D nanostructures. The above results stated clearly that the $_{3D}R^3$ nanostructure was obtained and the controllable formation between 2D and 3D could be successfully realized.

10.1002/anie.202010433

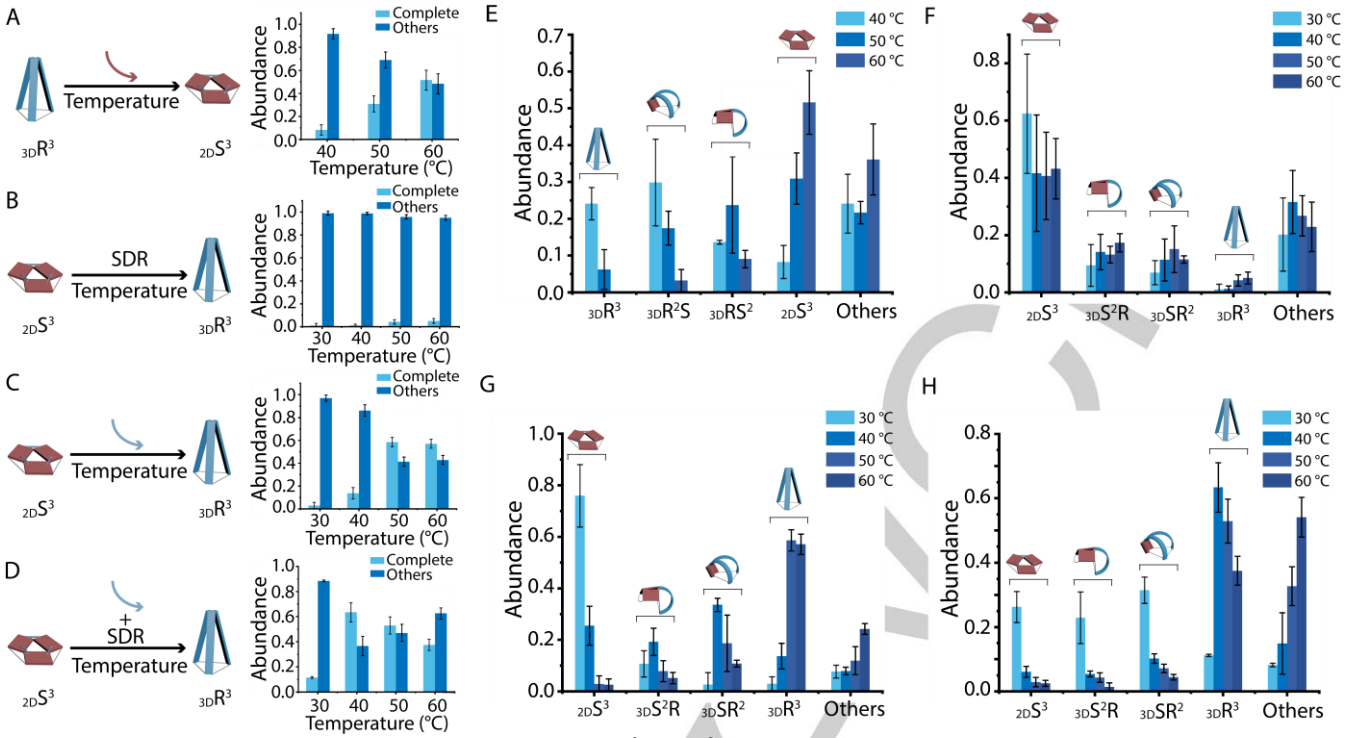

Figure 4. Controlled temperature transformation between the connected $_{2D}S^3$ and $_{3D}R^3$ DNA origami. (A) Controlled temperature transformation from the connected $_{3D}R^3$ to $_{2D}S^3$ DNA origami by red triggers and temperature, and transformation yield analysis. Controlled temperature transformation from the connected $_{2D}S^3$ to $_{3D}R^3$ through (B) toehold-mediated strand displacement reaction (SDR), (C) blue triggers, and (D) SDR and blue triggers-mediated reaction and its yield analysis. (E-H) Yield analysis of the modular transformation in (A-D) influenced by temperature. Others here meant the incomplete transformations of the structures.

To optimize the resettable structural transformation between the 2D and 3D connected DNA origami, the controllable temperature transformation strategy was employed (Figure 4). At first, the controllable temperature transformation from the $_{3D}R^3$ to $_{2D}S^3$ DNA origami was explored (Figure 4A). The $_{3D}R^3$ DNA origami was synthesized by annealing process, and then the controllable transformation from $_{3D}R^3$ to $_{2D}S^3$ DNA origami was performed by changing the incubation temperature. In Figure 4A, the optimum transformation temperature was 60 °C. Meanwhile, the yield of different nanostructures from $_{3D}R^3$ to $_{2D}S^3$ DNA origami was also calculated, and the yield of $_{2D}S^3$ DNA origami was nearly 60% (Figure 4E and Figure S50-S52). In addition, the controllable temperature transformation from the connected $_{2D}S^3$ to $_{3D}R^3$ DNA origami should be explored to realize the resettable structural transformation. Based on the design of the $_{2D}S^3$, the controlled transformation from $_{2D}S^3$ to $_{3D}R^3$ DNA origami could be realized via the toehold-mediated strand displacement reaction (SDR) and blue triggers-mediated reaction. At first, we applied SDR to realize the controlled transformation from $_{2D}S^3$ to $_{3D}R^3$ DNA origami. The red triggers here had a 10 nt toehold. When adding the complementary DNA strands (anti-triggers), the SDR could occur to release the red triggers (Figure S56), and the controlled transformation from $_{2D}S^3$ to $_{3D}R^3$ DNA origami could be realized. During the experiment, we found that the transformation efficiency was less than 10% (Figure 4B). Meanwhile, the yield of the different nanostructures during the transformation from $_{2D}S^3$ to $_{3D}R^3$ DNA origami demonstrated a similar result (Figure 4F and Figure S57-S60). The relatively low yield might be owing to the steric effect of tightened $_{2D}S^3$ DNA origami. To explore whether steric effect that influenced the transformation efficiency of tightened $_{2D}S^3$, we employed the $_{2D}S^3$ DNA origami without linkers to verify the transformation efficiency. The transformation efficiency from $_{2D}S^3$ to $_{2D}R^3$ was nearly 40% at 60 °C, indicating that the steric effect really influenced the transformation by SDR (Figure S68). Moreover, the controlled transformation efficiency was enhanced from $_{2D}S^3$ to $_{3D}R^3$ DNA origami by blue triggers-mediated reaction (yield nearly 60% at 50 °C in Figure 4C). Meanwhile, the yield of different nanostructures during the transformation from $_{2D}S^3$ to $_{3D}R^3$ DNA origami showed a similar result (Figure 4G and Figure S72-S75). Based on the design of the tightened $_{2D}S^3$, we could apply both SDR and blue triggers-mediated reaction simultaneously to realize the controlled transformation, which may improve the transformation efficiency. As seen in Figure 4D, the optimal transformation temperature was 40°C, which was lower than the SDR or blue triggers-mediated reaction. Meanwhile, the yield of different nanostructures during the transformation from $_{2D}S^3$ to $_{3D}R^3$ DNA origami was also calculated, and the yield of the $_{3D}R^3$ DNA origami was improved to over 60% at 40 °C (Figure 4H and Figure S80-S83). The above results indicated that the optimum controlled transformation between the $_{3D}R^3$ DNA origami and $_{2D}S^3$ DNA origami could be successfully realized.

Conclusion

In conclusion, we have shown a new strategy for constructing modular reconfigurable DNA nanostructures from 2D to 3D. To

demonstrate this, a 2D reconfigurable DNA origami sheet was constructed via the assembly of the anti-junction units. In addition, the 2D DNA origami sheet could be modularized into two, three and four parts, which could successfully realize the independent transformation between two conformations (e.g. rectangle to square conformation) driven by "trigger" DNA strands. What's more, the modular transformation of the connected 2D DNA origami sheet could be successfully achieved. Interestingly, the 2D connected modular reconfigurable DNA nanostructures could realize resettable transformation into 3D architectures owing to the shape change of the individual modules and the constraints induced by the connections between modules. This approach can provide an efficient mean efficiently for constructing programmable, higher-order, and complex DNA objects, and will offer fascinating possibilities for various applications.

Acknowledgements

The authors are grateful for the financial support from the National Natural Science Foundation of China (Nos. 81822024, 11761141006), the Natural Science Foundation of Shanghai, China (Nos. 19520714100, 19ZR1475800), the National Key Research and Development Program of China (Grant No. 2017YFC1200904), and the Project of Shanghai Jiao Tong University (2019QYA03 and YG2017ZD07).

Author Contributions

J.S. conceived the concept; J.S., Y.L., J.C. and Y.K. designed the experiments; Y.L. and J.C. performed the experiments; Y.L. and J.C. analyzed data and wrote the paper; S.F., H.G., T.L., L.T., B.J. and C.Z. commented the paper; All authors commented and revised the paper.

Keywords: Modular Reconfigurable DNA Origami • Modular Transformation • 2D to 3D

[1] N. C. Seeman, *J. Theor. Biol.* **1982**, *99*, 237-247.

[2] P. W. Rothemund, *Nature* **2006**, *440*, 297-302.

[3] A. Mangalum, M. Rahman, M. L. Norton, *J. Am. Chem. Soc.* **2013**, *135*, 2451-2454.

[4] a) C. Zhang, J. Yang, S. Jiang, Y. Liu, H. Yan, *Nano Lett.* **2016**, *16*, 736-741; b) M. Endo, Y. Yang, Y. Suzuki, K. Hidaka, H. Sugiyama, *Angew. Chem., Int. Ed.* **2012**, *51*, 10518-10522.

[5] a) A. Buchberger, C. R. Simmons, N. E. Fahmi, R. Freeman, N. Stephanopoulos, *J. Am. Chem. Soc.* **2020**, *142*, 1406-1416; b) E. S. Andersen, M. Dong, M. M. Nielsen, K. Jahn, R. Subramani, W. Mamdouh, M. M. Golas, B. Sander, H. Stark, C. L. Oliveira, J. S. Pedersen, V. Birkedal, F. Besenbacher, K. V. Gothelf, J. Kjems, *Nature* **2009**, *459*, 73-76.

[6] a) A. Kuzuya, Y. Sakai, T. Yamazaki, Y. Xu, M. Komiyama, *Nat. Commun.* **2011**, *2*, 449; b) D. J. Kauert, T. Kurth, T. Liedl, R. Seidel, *Nano Lett.* **2011**, *11*, 5558-5563.

[7] a) J. T. Powell, B. O. Akhuetie-Oni, Z. Zhang, C. Lin, *Angew. Chem., Int. Ed.* **2016**, *55*, 11412-11416; b) T. Tigges, T. Heuser, R. Tiwari, A. Walther, *Nano Lett.* **2016**, *16*, 7870-7874.

[8] a) A. J. Thubagere, W. Li, R. F. Johnson, Z. Chen, S. Doroudi, Y. L. Lee, G. Izatt, S. Wittman, N. Srinivas, D. Woods, E. Winfree, L. Qian, *Science* **2017**, *357, eaan6558* ; b) J. Li, A. Johnson-Buck, Y. R. Yang, W. M. Shih, H. Yan, N. G. Walter, *Nat. Nanotechnol.* **2018**, *13*, 723-729.

[9] a) S. M. Douglas, I. Bachelet, G. M. Church, *Science* **2012**, *335*, 831-834 ; b) G. Chatterjee, N. Dalchau, R. A. Muscat, A. Phillips, G. Seelig, *Nat. Nanotechnol.* **2017**, *12*, 920-927.

[10] a) T. Gerling, K. F. Wagenbauer, A. M. Neuner, H. Dietz, *Science* **2015**, *347*, 1446-1452 ; b) J. List, E. Falgenhauer, E. Kopperger, G. Pardatscher, F. C. Simmel, *Nat. Commun.* **2016**, *7*, 12414.

[11] a) J. Song, Z. Li, P. Wang, T. Meyer, C. Mao, Y. Ke, *Science* **2017**, *357, eaan3377* ; b) S. Fan, D. Wang, J. Cheng, Y. Liu, T. Luo, D. Cui, Y. Ke, J. Song, *Angew. Chem., Int. Ed.* **2020**, *59*, 12991-*12997* ; c) D. Wang, J. Song, P. Wang, V. Pan, Y. Zhang, D. Cui, Y. Ke, *Nat. Protoc.* **2018**, *13*, 2312-2329 ; d) S. Fan, J. Cheng, Y. Liu, D. Wang, T. Luo, B. Dai, C. Zhang, D. Cui, Y. Ke, J. Song, *J. Am. Chem. Soc*. **2020**, *142*, 14566-14573.

[12] a) Y. Choi, H. Choi, A. C. Lee, H. Lee, S. Kwon, *Angew. Chem., Int. Ed.* **2018**, *57*, 2811-2815; b) F. A. Aldaye, H. F. Sleiman, *J. Am. Chem. Soc.* **2007**, *129*, 13376-13377 ; c) Y. Zhang, X. Le, Y. Jian, W. Lu, J. Zhang, T. Chen, *Adv. Funct. Mater.* **2019**, *29*, 1905514.

[13] a) S. Modi, G. S. M, D. Goswami, G. D. Gupta, S. Mayor, Y. Krishnan, *Nat. Nanotechnol.* **2009**, *4*, 325-330; b) H. K. Walter, J. Bauer, J. Steinmeyer, A. Kuzuya, C. M. Niemeyer, H. A. Wagenknecht, *Nano Lett.* **2017**, *17*, 2467-2472.

[14] a) Q. Jiang, C. Song, J. Nangreave, X. Liu, L. Lin, D. Qiu, Z. G. Wang, G. Zou, X. Liang, H. Yan, B. Ding, *J. Am. Chem. Soc.* **2012**, *134*, 13396-13403 ; b) Q. Zhang, Q. Jiang, N. Li, L. R. Dai, Q. Liu, L. L. Song, J. Y. Wang, Y. Q. Li, J. Tian, B. Q. Ding, Y. Du, *ACS Nano* **2014**, *8*, 6633-6643.

[15] a) J. Chao, J. Wang, F. Wang, X. Ouyang, E. Kopperger, H. Liu, Q. Li, J. Shi, L. Wang, J. Hu, L. Wang, W. Huang, F. C. Simmel, C. Fan, *Nat. Mater.* **2019**, *18*, 273-279 ; b) K. Lund, A. J. Manzo, N. Dabby, N. Michelotti, A. Johnson-Buck, J. Nangreave, S. Taylor, R. Pei, M. N. Stojanovic, N. G. Walter, E. Winfree, H. Yan, *Nature* **2010**, *465*, 206-210 ; c) S. F. Wickham, J. Bath, Y. Katsuda, M. Endo, K. Hidaka, H. Sugiyama, A. J. Turberfield, *Nat. Nanotechnol.* **2012**, *7*, 169-173.

[16] a) A. E. Marras, L. Zhou, H. J. Su, C. E. Castro, *Proc. Natl. Acad. Sci. U. S. A.* **2015**, *112*, 713-718 ; b) Y. Yang, M. A. Goetzfried,

10.1002/anie.202010433

K. Hidaka, M. You, W. Tan, H. Sugiyama, M. Endo, *Nano Lett.* **2015**, *15*, 6672-6676.

[17] a) J. J. Funke, P. Ketterer, C. Lieleg, S. Schunter, P. Korber, H. Dietz, *Sci. Adv.* **2016**, *2*, e1600974 ; b) M. Iwaki, S. F. Wickham, K. Ikezaki, T. Yanagida, W. M. Shih, *Nat. Commun.* **2016**, *7*, 13715.

[18] a) H. Park, N. Heldman, P. Rebentrost, L. Abbondanza, A. Iagatti, A. Alessi, B. Patrizi, M. Salvalaggio, L. Bussotti, M. Mohseni, F. Caruso, H. C. Johnsen, R. Fusco, P. Foggi, P. F. Scudo, S. Lloyd, A. M. Belcher, *Nat. Mater.* **2016**, *15*, 211-216 ; b) I. H. Stein, C. Steinhauer, P. Tinnefeld, *J. Am. Chem. Soc.* **2011**, *133*, 4193-4195.

10.1002/anie.202010433

WILEY-VCH

Research articles

Entry for the Table of Contents

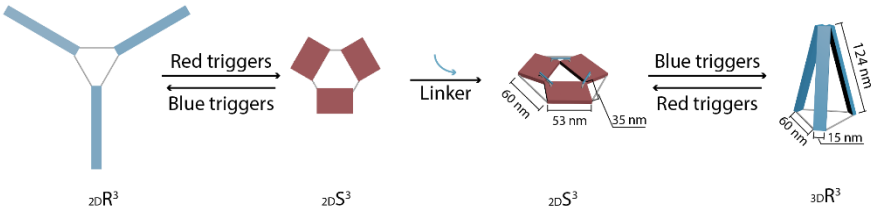

We demonstrated a new strategy for constructing modular reconfigurable DNA nanostructures from 2D to 3D. This strategy showed an efficient mean for constructing programmable, higher-order, and complex DNA objects, and potential applications, as well as sophisticated dynamic substrates for various applications.